

Confinement-induced Ultrafast Conductivity in 2D Perovskites resolved by correlative Terahertz-NIR Spectroscopy

Lion Krüger^{1#}, Fabian Brütting^{1,4#}, Michael Baumann², Moritz B. Heindl¹, Maximilian Spies³, Anna Köhler³, Alexander JC Kühne², Georg Herink^{1*}

¹ Experimental Physics VIII - Ultrafast Dynamics, University of Bayreuth, Bayreuth, Germany

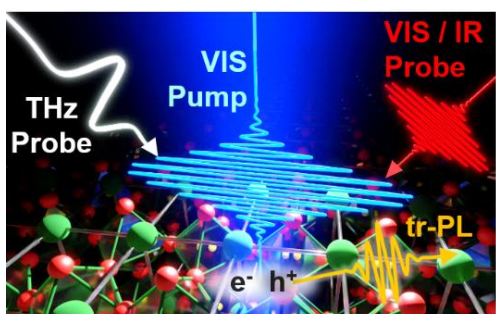
² Institute of Organic and Macromolecular Chemistry, Ulm University, Ulm, Germany

³ Soft matter Optoelectronics, Bayreuth Institute of Macromolecular Research (BIMF) and Bavarian Polymer Institute (BPI), University of Bayreuth, Bayreuth, Germany

⁴ School of Chemistry, The University of Melbourne, Parkville, Victoria, Australia

Co-first authors of this article

* Author to whom correspondence should be addressed: georg.herink@uni-bayreuth.de



Abstract: Quantum wells made of two-dimensional organic-inorganic hybrid perovskites (2D-PKs) offer a high degree of flexibility in tailoring optoelectronic properties through carrier confinement and functional interlayers. Compared to their 3D counterparts, 2D-PKs exhibit tunable photoluminescence, excitonic binding at room temperature and enhanced structural stability. However, the dynamics of photo-induced

charge carriers and their transport properties are highly intertwined due to the interplay of diverse excitation species, charge carrier cooling, transport, and radiative and non-radiative recombination. In this study, we employ optical-pump terahertz-probe spectroscopy (OPTP) to analyze the local conductivity dynamics of 2D and 3D methylammonium lead iodide (MAPI) perovskites at timescales down to picoseconds. Remarkably, we observe an intensity-dependent, 2D-specific buildup of an ultrafast, few-picosecond decay in local conductivity. By combining OPTP with transient absorption (TA) and picosecond time-resolved photoluminescence (TRPL), we demonstrate the disentanglement of photoconductivity and carrier population. This allows us to attribute the 2D-specific ultrafast THz response to delayed hot-carrier cooling and subsequent exciton formation, which effectively reduces the free-carrier conductivity. This intensity-dependent, ultrafast THz response is a signature of the recently identified hot-carrier bottleneck in 3D MAPI, and this effect manifests itself in a unique form in the 2D material. These results encourage further investigations on the impact of functional organic interlayers and provide insights into designing tunable carrier responses for ultrafast devices via adapted heterostructures and confinement.

I. INTRODUCTION

2D hybrid organic-inorganic perovskites (2D-PKs) represent an exciting alternative to classical inorganic materials, since they combine broadly tuneable optoelectronic semiconductor properties of hybrid perovskites with additional degree of freedom via highly anisotropic material compositions as well as dielectric and quantum confinement. 2D-PK quantum wells are solution processable and the stoichiometry between small methyl ammonium- (MA) and large organic ammonium-ions controls the active layer thickness n . The organic interlayers induce dielectric confinement, i.e. reduce Coulomb screening of electrons and holes in the PK

semiconductor and stabilize excitons at room temperature¹. In addition, 2D-PK exhibit superior resistance against ion migration and humidity compared to the 3D MAPI perovskite. Accordingly, 2D-PKs represent an attractive material system for next-generation photonic applications in micro-LEDs and lasers² and also as a protective additive in solution-processable solar cells^{3,4}.

Due to the complex photophysical response, insights into the primary steps of light-matter interaction and the nature of charge transport are highly intertwined. The intrinsic material features diverse charge carrier recombination channels, including debated hot carrier effects, exciton formation and transport⁵. On the other hand, the added structural and compositional degrees of freedom introduce novel degrees to engineer carrier dynamics⁶, and also render the material susceptible to inhomogeneities and varying degrees of confinements within the sample.

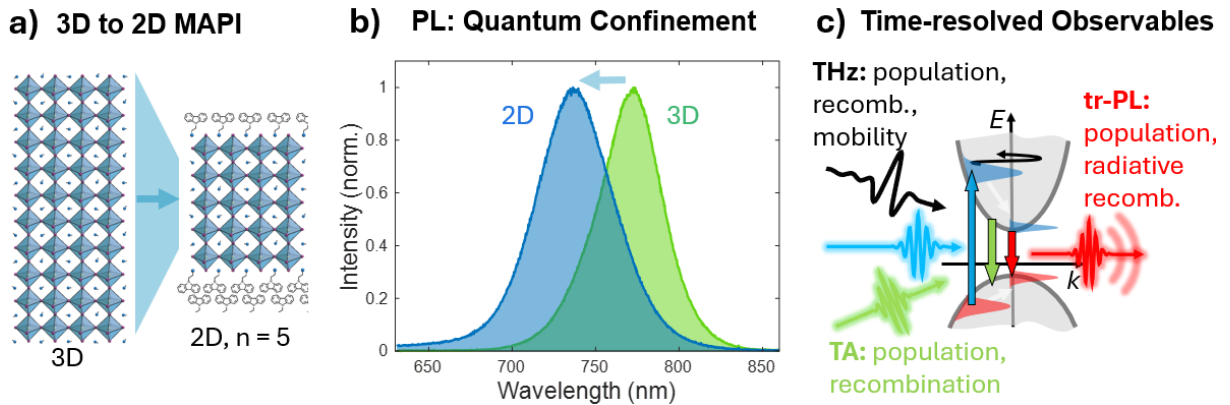


FIG 1: a) The impact of confinement from 3D MAPI to 2D quantum wells with layer thickness $n=5$ is studied. b) Photoluminescence spectra (PL) display a blue-shift due to the quantum confinement in 2D-MAPI. c) This study combines a set of time-resolved observables to access population and mobility dynamics: optical-pump THz-probe spectroscopy (OPTP), transient absorption (TA) and time-resolved photoluminescence (tr-PL).

Time-resolved Terahertz (THz) spectroscopy in combination with near-infrared (NIR) and visible (VIS) transient absorption and photoluminescence spectroscopy has recently been established for non-contact access to initial photo-induced carrier and conductivity dynamics in hybrid perovskite materials^{6–10}. Previous transient absorption studies could resolve a remarkably slow, intensity-dependent cooling of hot carriers for above-bandgap excitation compared to conventional semiconductors^{11,12}. The effect has been attributed to a “hot phonon” bottleneck (HPB) with the buildup of a hot phonon population and the saturation of efficient carrier cooling via reduced phonon-phonon scattering^{11,13}. The dynamics have been also related to polaron formation in the soft ionic lattice¹⁴ and reduced electron-phonon coupling due to potential screening of the underlying Fröhlich interaction¹¹.

The impact of confinement on these complex charge carrier dynamics in the emerging class quantum-confined perovskites currently poses fundamental and unresolved questions. Interestingly, recent studies report two cooling regimes and an enhanced phonon bottleneck effect^{15–17}, but also the absence of an intensity-dependent phonon bottleneck effect for 2D-PKs¹⁸ – pointing towards a sensitive dependence of carrier relaxation on the specific 2D material. Quantum confinement generally enhances early bimolecular and Auger recombination channels¹⁹. Furthermore, THz-studies report a reduced trap-related recombination¹⁹ and

moderate to high mobilities for the anisotropic 2D sheet conductivity with respect to the 3D material^{20,21}. Yet, interactions with the organic interlayers add further complexity to the photophysical response but thereby open-up diverse avenues to modify the material response²¹ and design future optoelectronic function in well-controlled morphologies.

In this work, we investigate the impact of structural confinement onto photoinduced charge carrier dynamics and mobility for prototypical 2D MAPI thin films against the 3D material, as illustrated in Figure 1. We probe the material systems with combined time-resolved THz, transient absorption and ultrafast photoluminescence spectroscopy to gain access to the dynamics of photogenerated charge carriers and local conductivity.

II. EXPERIMENTAL METHODS

A. Ultrafast time-resolved THz/NIR/VIS spectroscopy

We access the evolution of carrier population, local conductivity and luminescence emission by combining a set of correlative time-resolved ultrafast spectroscopies, including optical-pump Terahertz-probe spectroscopy (OPTP), visible/near-infrared transient absorption (TA) and picosecond temporally-resolved photoluminescence (tr-PL).

Optical-pump Terahertz-probe spectroscopy (OPTP) is based on an Ytterbium-based femtosecond amplifier system (Light conversion, Pharos) with 150-fs pulses at an energy of 1 mJ and repetition rate of 10 kHz. The generation of single-cycle THz pulses at 1 THz is based on optical rectification in LiNbO₃ in the tilted-pulse front phase-matching geometry, as described in Ref. (22). Second harmonic generation (SHG) of a fraction of the laser fundamental generates visible pump pulses at 515 nm. Pump and THz pulses are co-focused onto the sample. THz-pulses are detected via electro-optical sampling employing the Pockels effect in a 1 mm-GaP crystal. Sampling pulses are generated by an optical-parametric amplifier (OPA) that is pumped with a small fraction of the laser amplifier. The pump pulses are chopped for sensitive lock-in detection.

Transient absorption spectroscopy in the visible/near-infrared spectrum is implemented via the SHG-based pump pulses and tunable probing pulses from the OPA. The probe wavelength is tuned to the minimum of the conduction band / exciton transition of 750 nm and 720 nm of 3D/2D MAPI, respectively.

Time-resolved photoluminescence spectra (tr-PL) have been acquired with a streak-camera / spectrograph combination (Hamamatsu C5680, Synchro-Scan) with a temporal resolution down to < 10 ps. The samples have been excited with SHG ($\lambda = 415$ nm) of an actively-modelocked Ti:Sapphire oscillator with a repetition rate of 80 MHz.

B. Material synthesis

The synthetic details of the 2D quantum wells are described in the Supporting Information. In short, we prepare stoichiometric solutions of the respective perovskite precursors ($n = 5$, $n = \infty$) in a mixture of DMF and DMSO (1:1). The solutions are spin coated on quartz substrates, where

perovskite formation is induced by applying chlorobenzene as an antisolvent. The obtained films are baked at 100 °C and then exposed to methyl amine gas to obtain 377±47 nm thick 2D films. The final films are encapsulated with a layer of PMMA.

To prepare the 3D perovskite, we mix lead acetate trihydrate (PbOAc_2) and methylammonium iodide (MAI) in a molar ratio of 1:3 in DMF at a concentration of 0.7 mol/L. The solution was stirred overnight, and the incorporation of a small amount (<15%) of dimethylammonium cannot be excluded²³. The solutions were then spin coated on quartz substrates (without antisolvent) and annealed at 150°C for 10 minutes to yield films of 230 nm. Subsequently, the final films are encapsulated with a layer of PMMA.

III. EXPERIMENTAL RESULTS AND DISCUSSION

A. Initial Picosecond Response

First, we focus on the early phase of THz-conductivity in 3D and 2D after photoexcitation above band gap. Figure 2 presents corresponding OPTP (black) and TA traces (photobleach (PB), green) for excitation fluences between 30 to 500 $\mu\text{J}/\text{cm}^2$. The optical transmission increases upon excitation, due to the photobleach, which probes carrier relaxation and population at the conduction band minimum. The THz transmission decreases upon photocarrier generation proportional to the local conductivity, given by the product of the number of carriers and their mobility^{24,25}. The full dataset tracks characteristic evolutions and resolves specific differences between 3D and 2D-MAPI.

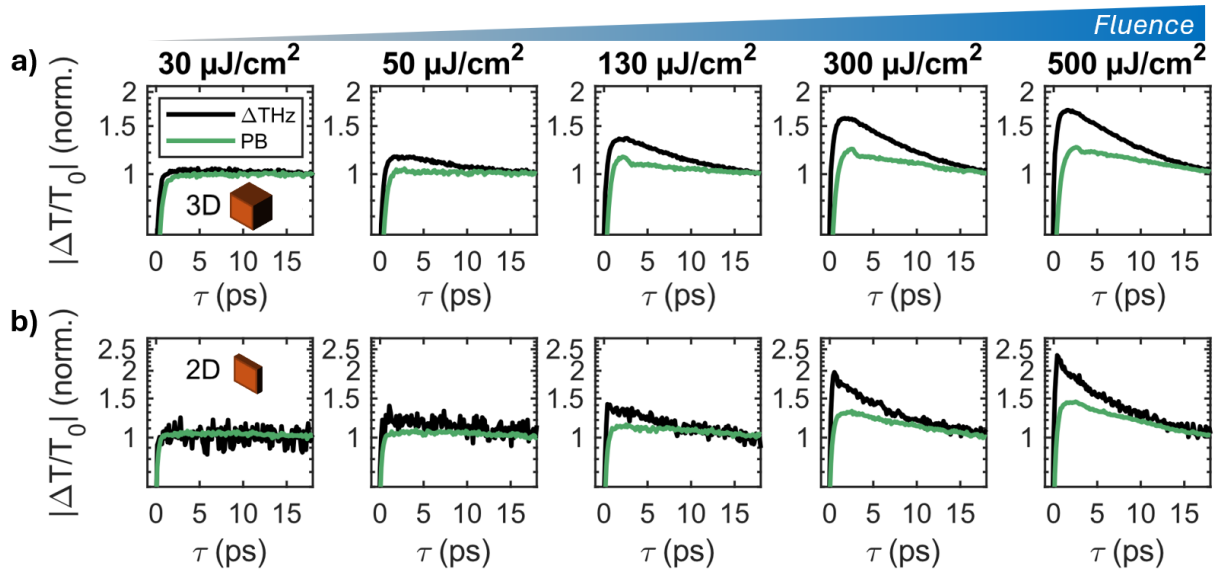


FIG 2: Early phases of carrier dynamics (photobleach (PB, green)) and THz-transmission (black) for 3D and 2D MAPI. For better comparison, we present absolute (unsigned) values. Excitation fluences increase from 30 to 500 $\mu\text{J}/\text{cm}^2$.

To facilitate the comparison, we now discuss the data in a reduced representation based on two limiting (lowest and highest) fluences: As displayed in Fig 3a), 3D-MAPI exhibits a maximum in the THz conductivity after a delay of ~1-2 ps without shifting for higher fluence, as indicated by the blue arrow. In contrast, the onset of the photobleach (PB) at band gap temporally shifts

with higher excitation (light red arrow). Figure 3b) illustrates the 3D carrier dynamics: at low intensity, fast cooling (dashed lines) results in a quasi-instantaneous photobleach signal due to efficient energy dissipation via electron-phonon and phonon-phonon coupling. In addition to carrier population, THz radiation probes the carrier mobility: the THz-absorption signal exhibits a maximum *before* the maximum of the PB signal, i.e. during the carrier cooling. Such behaviour can be related to non-parabolicity in the bands of MAPI, resolved during the cooling process²¹. Notably, broad hot carrier distributions contribute to the THz signal during carrier cooling and the deviations between the slopes of PB and THz can be attributed to the admixture of faster decaying higher levels, as observed in Ref.¹². At high intensity excitation, sketched in Fig. 2b, the fluence-dependent delay in the PB can be attributed to the hot phonon bottleneck (HPB), as reported for MAPI in various previous studies^{11,12,18,13}. The HPB effect prolongs cooling times up to several ps for carrier densities around 10^{18} cm^{-3} .

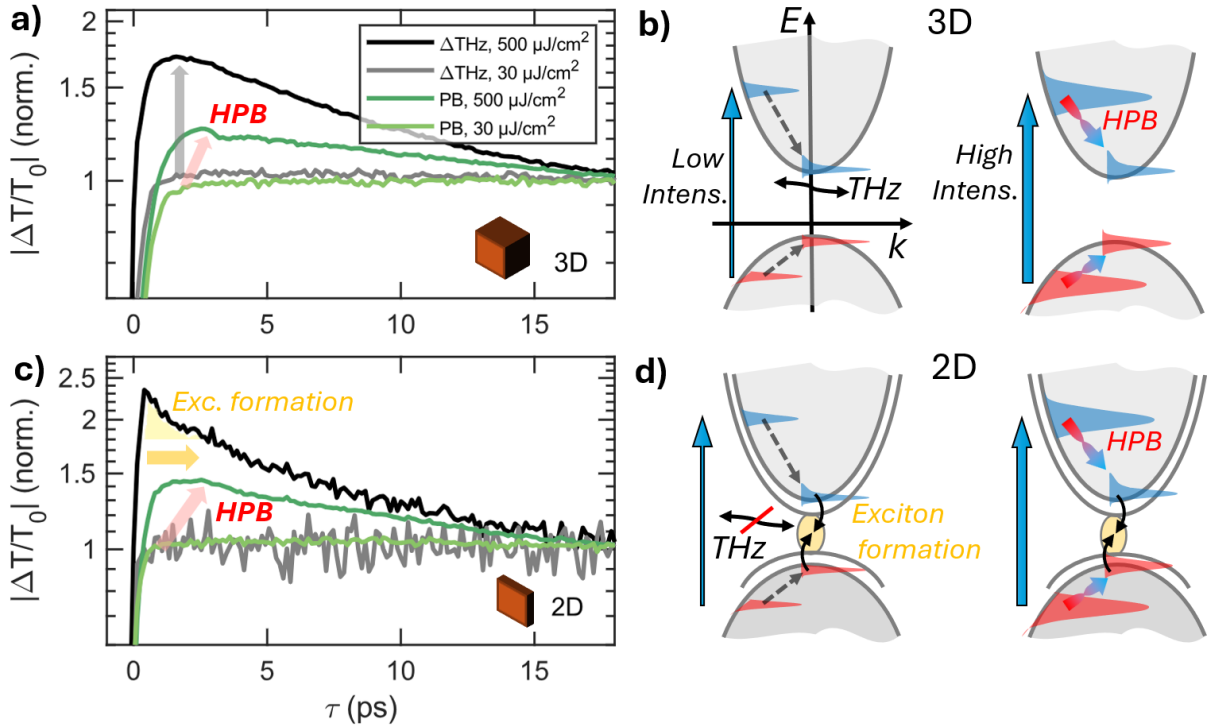


FIG 3: Early phases of carrier dynamics and THz-conductivity for 3D and 2D at low/high intensities: a) 3D-MAPI exhibits maximum THz conductivity (grey/black) at a picosecond delay without shift for high intensities (grey arrow). In contrast, the photo bleach at band gap (PB, green) delays at higher excitation due to the hot phonon bottleneck (HPB, red arrow). b) Illustration of the 3D carrier dynamics in the two regimes; the dashed lines indicate cooling due to electron-phonon scattering. THz probes carrier population and mobility. c) The PB signals in 2D-MAPI delays for increasing intensity - comparable to 3D. Yet, for high intensity, an additional 2D-specific ultrafast THz onset and decay builds-up (orange shaded). The feature coincides with the hot phonon bottleneck. d) In 2D, photocarriers can form excitons upon cooling; such bound electron-hole pairs reduce THz absorption. At high excitation, however, the reduced cooling (see PB, red arrow) delays exciton formation and, thus, yields the intensity-dependent transient THz-decay.

We now compare the 3D-signals with corresponding data from 2D-MAPI in Fig 3c: the PB signals exhibit comparable shifts akin to the 3D-HPB effect for increasing intensity. Remarkably, however, the THz-conductivity exhibits a characteristic 2D-specific ultrafast onset

of THz-conductivity with an additional rapid decay which builds-up for high intensities, as indicated in Fig. 3c. This ultrafast 2D-feature coincides with the hot phonon bottleneck (orange arrow). We attribute this observation to the confinement-induced enhanced exciton binding energy in the 2D-PK: Illustrated in Fig. 3d, free hot electrons and holes can form excitons *during* the cooling process - given the high exciton binding energies exceeding 100-200 meV for the 2D-PK via reduced screening of electric fields inside the layered dielectric structure. “Exciton states” have been added to the single-electron bulk diagram in Fig. 4d. Such bound electron-hole pairs are electrically neutral and exhibit negligible THz absorption outside their resonance. Thus, they generate an additional decay channel for electronic conductivity. The fraction of excitons to free electron-holes follows equilibrium dynamics similar to the Saha description in plasma physics, however, significantly modified in the solid state – yielding fractions of several 10% at room temperature, as recently discussed^{20,21}. For low fluence, the fast carrier cooling and exciton formation instantaneously reduces the maximum conductivity. For high excitation, however, the reduced cooling (see PB, red arrow) delays exciton formation and, thus, induces an intensity-dependent ultrafast THz-decay feature. We note that picosecond decays have been observed in few THz-studies – but, independent on intensity for above-bandgap excitation and not corresponding to the HPB signal in PB^{20,21,26} to our knowledge. Finally, the HPB has not been observed for 2D-PK in Ref.¹⁸, however, data was recorded for isolated nanoplatelets in solution. Such differences might arise from dissimilar confinement strength, i.e. n-values, and the interlayer composition. In addition, a related effect might have been exploited for ultrafast THz photonic devices, however, the intensity-resolved data does not allow for a certain interpretation²⁷.

B. Intermediate Sub-Nanosecond Response

Next, we evaluate the intermediate carrier dynamics on timescales of several-100 ps. Figure 4 displays correlative time-resolved signals from OPTP, TA and PL for two different excitation fluences. For 3D MAPI, the PB (green) and OPTP (black) signals exhibit essentially identical dynamics after the initial carrier cooling is completed within ~20 ps, as presented in Figs.4a,c. Hence, the decay of THz-conductivity can be attributed predominantly to the dynamics of the carrier population at the conduction band minimum. In addition, we include the photoluminescence (tr-PL) trace. The underlying tr-PL-spectra are obtained with a streak-camera/spectrograph combination. The traces were integrated over 30 nm around the peak wavelength, and they are presented as the square root signal of the measured intensity since the bimolecular radiative recombination follows $\propto k_2 n^2$ with carrier density n of a direct bandgap semiconductor. In fact, these overall PL dynamics also mirror the population decay for longer timescales. Differences at early times might be attributed to the impulse response function (~10 ps) and to an excitation wavelength which is blue-shifted compared to the OPTP data, i.e. 415 nm vs. 515 nm.

For 2D, all OPTP, BP and PL traces also resolve an identical evolution at lower fluence, as shown in Fig.4b. Intriguingly, however, for higher intensity, OPTP and BP reveal different decays at intermediate decays around 200 ps. Such differences might present a hallmark of additional (multi-)excitonic decay channels at high intensities, i.e. bi-excitonic and Auger

recombination. Such recombination directly reduces the excitonic parts of the population and luminescence dynamics with reduced impact onto the free-carrier THz absorption.

Finally, we present extended sets of OPTP traces in the Supporting Information, and we extracted photophysical rate constants using global fitting after the initial carrier cooling phase. Despite subject to the typical high uncertainties, the bimolecular “excitonic” recombination (rate constant k_2) appears significantly enhanced and dominating for the 2D material - in line recent complimentary spectroscopic results²⁸. We note that, in particular for 3D, diffusion along the excitation gradient introduces an additional component to the dynamics. Future correlative measurements will benefit from the addition of sensitive, spatially resolved measurements²⁹.

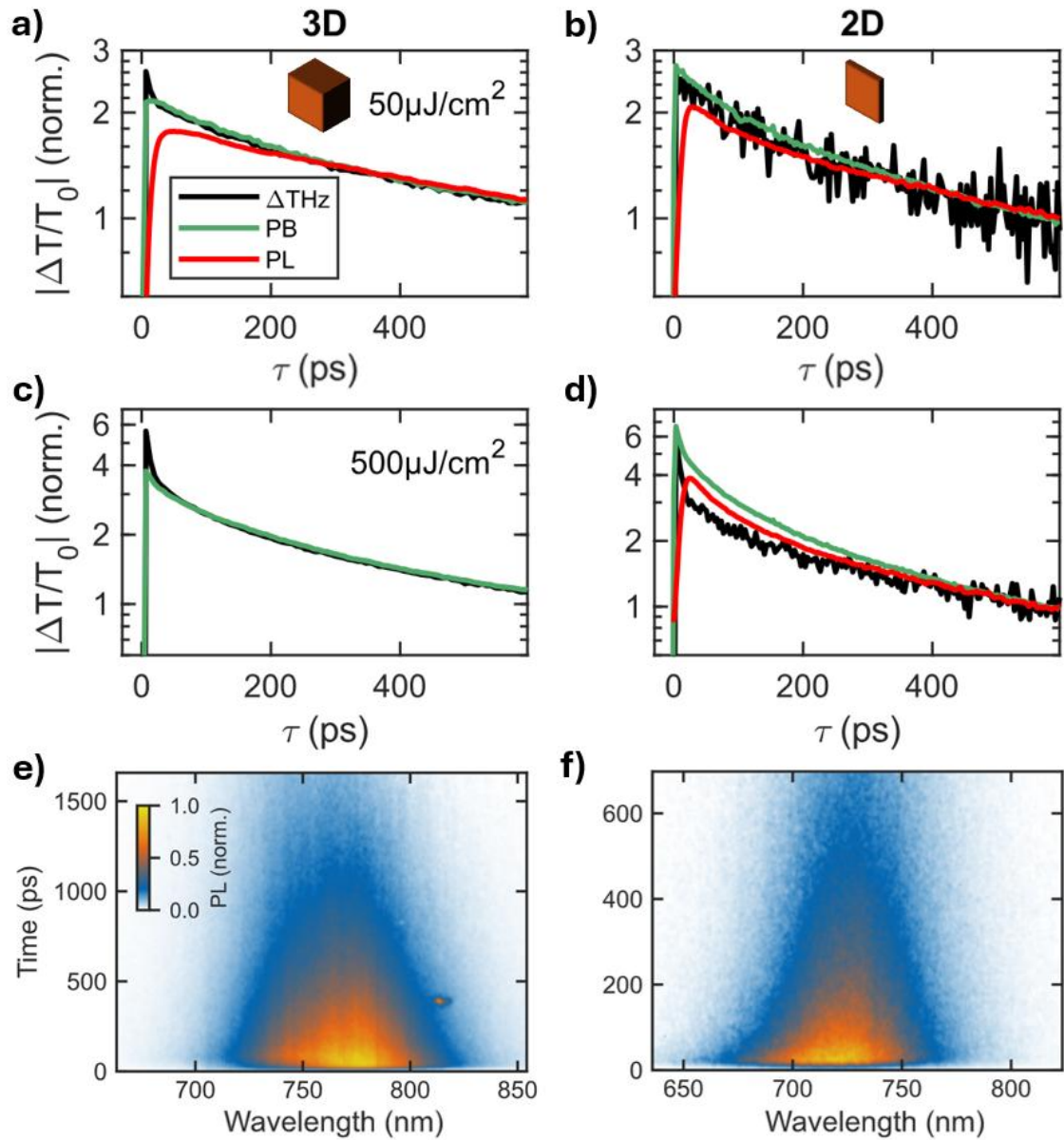


FIG 4: Correlative time-resolved signals in the intermediate phase of carrier dynamics for 3D and 2D. a,b) Photobleach (PB, green), THz conductivity (black) and photoluminescence (PL, red) for 3D and 2D MAPI. The PL is included as the square root of the intensity. c,d) Signals at increased intensity. e,f) Characteristic PL streaking traces, recorded at 50 $\mu\text{J}/\text{cm}^2$.

IV. CONCLUDING REMARKS

In this study, we investigate the confinement of 3D hybrid perovskite films to 2D on the initial stages of charge carrier generation and transport, using correlative ultrafast spectroscopic techniques covering the NIR and THz spectrum. Combining time-resolved THz spectroscopy with transient absorption and photoluminescence spectroscopy provides access to the dynamics of photo-generated carrier species, populations and mobility in the picosecond to nanosecond range. Specifically, we observe an intensity-dependent picosecond transient in the carrier population of the 2D material that features the signature of a “hot phonon” bottleneck. While this effect has been observed in various 3D hybrid perovskites, the THz conductivity exhibits an accelerated 2D-feature specific that has not previously been reported to our knowledge. We attribute the ultrafast conductivity decay to the delayed formation of excitons caused by the blocked cooling of hot carriers. This correlative dataset sheds light on the critical interplay between electronic conductivity, hot carrier dynamics with electron-phonon and phonon-phonon interactions, and exciton formation. Further applications of this approach promise to reveal the active role of functional organic interlayers and provide insights into the rational design of tunable, ultrafast carrier responses for future optoelectronic devices.

ACKNOWLEDGMENTS

We thank J. Köhler for supporting the study with the streak camera setup.

This work was supported by the German Research Foundation (DFG) via CRC 1585 “Structured functional materials for multiple transport in nanoscale confinements”, project number 492723217 and projects 403711541, 445471845, 445471097, 445470598.

F.B. acknowledges financial support by the German Research Foundation (DFG) via IRTG 2818 (OPTEXC) and by the Elite Network of Bavaria (study program Biological Physics).

AUTHOR CONTRIBUTIONS

GH and AJCK devised, planned, and supervised the study. LK, FB designed the OPTP and PB experiments, acquired and processed the data. FB acquired and processed the tr-PL data. LK and FB are co-first authors of this article. MB synthesized the 2D samples, acquired structural data and steady-state optical characterizations. MBH designed the OPTP experiment and acquired tr-PL data. MS, supervised by AK, synthesized the 3D samples and acquired structural data. All authors contributed to the discussion, analysis of the results and writing of the manuscript.

REFERENCES

1. Hansen, K. R., Colton, J. S. & Whittaker-Brooks, L. Measuring the Exciton Binding Energy: Learning from a Decade of Measurements on Halide Perovskites and Transition Metal Dichalcogenides. *Adv. Opt. Mater.* **12**, 2301659 (2024).
2. Chen, Y. *et al.* 2D Ruddlesden–Popper Perovskites for Optoelectronics. *Adv. Mater.* **30**, 1703487 (2018).
3. Chen, P. *et al.* In Situ Growth of 2D Perovskite Capping Layer for Stable and Efficient Perovskite Solar Cells. *Adv. Funct. Mater.* **28**, 1706923 (2018).
4. Lee, J.-W. *et al.* 2D perovskite stabilized phase-pure formamidinium perovskite solar cells. *Nat. Commun.* **9**, 3021 (2018).
5. Fu, J., Ramesh, S., Melvin Lim, J. W. & Sum, T. C. Carriers, Quasi-particles, and Collective Excitations in Halide Perovskites. *Chem. Rev.* **123**, 8154–8231 (2023).
6. Boeije, Y. *et al.* Molecular Engineering of Interlayer Exciton Delocalization in 2D Perovskites. *J. Am. Chem. Soc.* **147**, 31541–31557 (2025).
7. Jepsen, P. u., Cooke, D. g. & Koch, M. Terahertz spectroscopy and imaging – Modern techniques and applications. *Laser Photonics Rev.* **5**, 124–166 (2011).
8. Lloyd-Hughes, J. & Jeon, T.-I. A Review of the Terahertz Conductivity of Bulk and Nano-Materials. *J. Infrared Millim. Terahertz Waves* **33**, 871–925 (2012).
9. Johnston, M. B. & Herz, L. M. Hybrid Perovskites for Photovoltaics: Charge-Carrier Recombination, Diffusion, and Radiative Efficiencies. *Acc. Chem. Res.* **49**, 146–154 (2016).
10. Herz, L. M. Charge-Carrier Mobilities in Metal Halide Perovskites: Fundamental Mechanisms and Limits. *ACS Energy Lett.* **2**, 1539–1548 (2017).
11. Neu, J. Optical Pump Terahertz Probe (OPTP) and Time Resolved Terahertz Spectroscopy (TRTS) of emerging solar materials. *APL Photonics* **8**, 071103 (2023).
12. Price, M. B. *et al.* Hot-carrier cooling and photoinduced refractive index changes in organic–inorganic lead halide perovskites. *Nat. Commun.* **6**, 8420 (2015).
13. Yang, J. *et al.* Acoustic-optical phonon up-conversion and hot-phonon bottleneck in lead-halide perovskites. *Nat. Commun.* **8**, 14120 (2017).
14. Faber, T., Filipovic, L. & Koster, L. J. A. The Hot Phonon Bottleneck Effect in Metal Halide Perovskites. *J. Phys. Chem. Lett.* **15**, 12601–12607 (2024).
15. Brenner, T. M. *et al.* Are Mobilities in Hybrid Organic–Inorganic Halide Perovskites Actually “High”? *J. Phys. Chem. Lett.* **6**, 4754–4757 (2015).
16. Lin, W. *et al.* Combining two-photon photoemission and transient absorption spectroscopy to resolve hot carrier cooling in 2D perovskite single crystals: the effect of surface layer. *J. Mater. Chem. C* **10**, 16751–16760 (2022).
17. Li, H. *et al.* Enhanced Hot-Phonon Bottleneck Effect on Slowing Hot Carrier Cooling in Metal Halide Perovskite Quantum Dots with Alloyed A-Site. *Adv. Mater.* **35**, 2301834 (2023).
18. Thompson, J. J. P. *et al.* Phonon-Bottleneck Enhanced Exciton Emission in 2D Perovskites. *Adv. Energy Mater.* **14**, 2304343 (2024).
19. Hintermayr, V. A., Polavarapu, L., Urban, A. S. & Feldmann, J. Accelerated Carrier Relaxation through Reduced Coulomb Screening in Two-Dimensional Halide Perovskite Nanoplatelets. *ACS Nano* **12**, 10151–10158 (2018).

20. Milot, R. L. *et al.* Charge-Carrier Dynamics in 2D Hybrid Metal–Halide Perovskites. *Nano Lett.* **16**, 7001–7007 (2016).
21. Kober-Czerny, M. *et al.* Excellent Long-Range Charge-Carrier Mobility in 2D Perovskites. *Adv. Funct. Mater.* **32**, 2203064 (2022).
22. Motti, S. G. *et al.* Exciton Formation Dynamics and Band-Like Free Charge-Carrier Transport in 2D Metal Halide Perovskite Semiconductors. *Adv. Funct. Mater.* **33**, 2300363 (2023).
23. Heindl, M. B. *et al.* Ultrafast imaging of terahertz electric waveforms using quantum dots. *Light Sci. Appl.* **11**, 5 (2022).
24. Franssen, W. M. J., Bruijnaers, B. J., Portengen, V. H. L. & Kentgens, A. P. M. Dimethylammonium Incorporation in Lead Acetate Based MAPbI₃ Perovskite Solar Cells. *ChemPhysChem* **19**, 3107–3115 (2018).
25. Nienhuys, H.-K. & Sundström, V. Intrinsic complications in the analysis of optical-pump, terahertz probe experiments. *Phys. Rev. B* **71**, 235110 (2005).
26. Ulbricht, R., Hendry, E., Shan, J., Heinz, T. F. & Bonn, M. Carrier dynamics in semiconductors studied with time-resolved terahertz spectroscopy. *Rev. Mod. Phys.* **83**, 543–586 (2011).
27. Balogun, F. H. *et al.* Untangling free carrier and exciton dynamics in layered hybrid perovskites using ultrafast optical and terahertz spectroscopy. *Mater. Res. Express* **11**, 025503 (2024).
28. Kumar, A. *et al.* Excitons in 2D perovskites for ultrafast terahertz photonic devices. *Sci. Adv.* **6**, eaax8821 (2020).
29. Nuber, M. *et al.* Bimolecular Generation of Excitonic Luminescence from Dark Photoexcitations in Ruddlesden–Popper Hybrid Metal–Halide Perovskites. *J. Phys. Chem. Lett.* **12**, 10450–10456 (2021).
30. Hörmann, M. *et al.* High-Sensitivity Visualization of Ultrafast Carrier Diffusion by Wide-Field Holographic Microscopy. *Ultrafast Sci.* **3**, 0032 (2023).